

22 **Abstract**

23 Degree-day factors are widely used to estimate snowmelt runoff in operational
24 hydrological models. Usually, they are calibrated on observed runoff, and sometimes on
25 satellite snow cover data. In this paper, we propose a new method for estimating the snowmelt
26 degree-day factor (DDF_s) directly from MODIS snow covered area (SCA) and ground-based
27 snow depth data without calibration. Subcatchment snow volume is estimated by combining
28 SCA and snow depths. Snow density is estimated as the ratio between observed precipitation
29 and changes in the snow volume for days with snow accumulation. Finally, DDF_s values are
30 estimated as the ratio between changes in the snow water equivalent and difference between
31 the daily temperature and the melt threshold value for days with snow melt. We compare
32 simulations of basin runoff and snow cover patterns using spatially variable DDF_s estimated
33 from snow data with those using spatially uniform DDF_s calibrated on runoff. The runoff
34 performances using estimated DDF_s are slightly improved, and the simulated snow cover
35 patterns are significantly more plausible. The new method may help reduce some of the
36 runoff model parameter uncertainty by reducing the total number of calibration parameters.
37 This method is applied to the Lienz catchment in East Tyrol, Austria, which covers an area of
38 1198 km². Approximate 70% of the basin is covered by snow in the early spring season.

39 1 Introduction

40 Mountain watersheds serve as important water sources by providing fresh water for
41 downstream human activities (Viviroli *et al.*, 2003; Langston *et al.*, 2011). As a result of
42 snow and glacier melt, the magnitude and timing of runoff from these watersheds tend to be
43 very sensitive to changes in the climate (Immerzeel *et al.*, 2009; Jeelani *et al.*, 2012). Changes
44 of melt runoff may even affect the sustainable development of downstream cities in the long
45 run (Verbunt *et al.*, 2003; Zhang *et al.*, 2012). Modeling snow and glacier melt runoff
46 processes is therefore quite important for local water supply, hydropower management and
47 flood forecasting (Klok *et al.*, 2001). However, melt runoff modeling in such regions faces
48 two challenges: scarcity of meteorological data and uncertainty in parameter calibration due
49 to limited understanding of the complex hydrological processes.

50 Melt runoff models generally fall into two categories: energy balance models, and
51 temperature-index models (Rango and Martinec, 1979; Howard, 1996; Kane *et al.*, 1997;
52 Singh *et al.*, 2000; Fierz *et al.*, 2003). Temperature-index models operating on a basin wide
53 scale are much more popular for operational purposes due to the following four reasons
54 (Hock, 2003): (1) wide availability of air temperature data, (2) relatively easy interpolation
55 and forecasting possibilities of air temperature, (3) generally good model performance and (4)
56 computational simplicity. The temperature index model is based on an assumed relationship
57 between ablation and air temperature and calculates the daily snowmelt depth, M (mm/d), by
58 multiplying the difference between daily temperature and the melt threshold value, $T - T_o$ ($^{\circ}\text{C}/$
59 d), with the degree-day factor of snow, DDF_s (mm/d/ $^{\circ}\text{C}$) (Howard, 1996). T_o is a threshold
60 temperature for snowmelt. The temperature index model implies a consistent contribution of
61 each of the heat balance components (including radiation, sensible heat, latent heat and
62 ground heat fluxes). Any changes in climate conditions and the underlying basin
63 characteristics will affect the relative contributions of the heat balance components and cause
64 variations of the DDF_s (Lang and Braun, 1990; Ohmura, 2001). The study of Kuusisto (1980)
65 in Finland found DDF_s to increase sharply in early April, approximately doubling during this
66 month due to increasing solar radiation. Singh and Kumar (1996) and Singh *et al.* (2000)
67 demonstrated a seasonal decrease of DDF_s with increasing albedo due to seasonal changes of

68 land surface characteristics. Spatial variations of basin topography, such as elevation, terrain
69 slope, aspect and terrain shading change the spatial energy conditions for snowmelt and lead
70 to significant variations of DDF_s (Marsh *et al.*, 2012; Bormann *et al.*, 2014). Generally,
71 regions with a large contribution of sensible heat flux to the heat balance tend to have low
72 degree-day factors (Hock, 2003). DDF_s are expected to increase with increasing elevation and
73 increasing snow density (Li and Williams, 2008). Forest regions often have lower values of
74 DDF_s than open regions (Rango and Martinec, 1995). The identification of DDF_s has been an
75 important yet complex issue for the application of the temperature-index model for snowmelt
76 runoff modeling.

77 Quite a few studies estimated the degree-day factor from observed snow water
78 equivalent (SWE) data. Martinec (1960) measured SWE with radioactive cobalt and
79 computed the DDF_s as the ratio between SWE and difference between daily temperature and
80 the melt threshold value. Rango and Martinec (1979, 1995) obtained degree-day factors from
81 empirical regressions with snow density. Kane *et al.* (1997) estimated degree-day factors by
82 calibration against point-measured SWE in a 2.2 km² catchment. Daly *et al.* (2000) merged
83 interpolated point-measured SWE with snow covered area derived from satellite data to
84 obtain spatial snow water equivalent and estimated spatially distributed DDF_s by calibration
85 to spatial snow water equivalent. Bormann *et al.* (2013, 2014) coupled the method developed
86 by Sturm *et al.* (2010) to estimate snow density as the ratio between point-measured SWE and
87 snow depth data with the empirical relationship between DDF_s and snow density of Rango
88 and Martinec (1995) to estimate daily variable DDF_s. In these methods, detailed observations
89 of snow water equivalent in the basin are needed. However, observations of snow water
90 equivalent are only representative of a small subset of the spatial domain, and observations
91 tend to be scarce at high elevations (Hamlet *et al.*, 2005).

92 Another method of estimating the DDF_s is treating it as a hydrologic model parameter
93 and calibrating it on observed hydrological data. Most commonly, runoff is used for
94 calibrating DDF_s (Hinzman and Kane, 1991; Klok *et al.*, 2001; Luo *et al.*, 2013). The
95 drawback is that catchment runoff is not usually a good indicator of the spatial snow cover
96 distribution (Blöschl *et al.*, 1991a,b; Bach *et al.*, 2003; Liu *et al.*, 2012 etc.). Advances in
97 remotely sensing techniques help provide more practical information for the calibration of

98 DDF_s. There have been numerous comparisons between satellite snow cover products (e.g.
99 Hall *et al.*, 2000, 2002; Maurer *et al.*, 2003; Lee *et al.*, 2005; Hall and Riggs, 2007). In
100 particular, MODIS snow covered area (SCA) products have been demonstrated to be of good
101 quality and have been widely used in alpine hydrological modeling (Klein and Barnett, 2003;
102 Dery *et al.*, 2005; Andreadis and Lettenmaier, 2006; Wang *et al.*, 2008; Georgievsky, 2009).
103 Subsequently, a number of studies tested the potential of MODIS snow cover data for
104 calibrating and validating snowmelt models (e.g. Dery *et al.* (2005), Tekeli *et al.* (2005),
105 Udnaes *et al.* (2007), Parajka and Blöschl (2008a)). A review is provided by Parajka and
106 Blöschl (2012). The authors generally found that including snow cover data in the model
107 calibration improved the snow simulations. Most of these studies calibrated the DDF_s on
108 combined objective functions involving observed runoff and snow cover data. This makes it
109 hard to obtain spatially variable DDF_s because of the limited availability of spatially
110 distributed runoff data. It is also important to note that the calibration of DDF_s can be
111 significantly affected by other model parameters due to the interdependency of the parameters
112 and the nature of objective functions that reflect the joint effects of all the model parameters
113 in a holistic way. The optimization procedures may there induce significant uncertainties in
114 the parameter estimates (Kirchner, 2006), if insufficient attention is paid to the physical
115 catchment characteristics (including elevation, vegetation coverage, and snow density etc.)
116 affecting the value of DDF_s (Bormann *et al.*, 2014).

117 In mountain watersheds, distributed hydrologic models are more widely applied than
118 lumped models due to the large spatial variability. Degree-day factors estimated from point
119 measurements or spatially uniform values from calibration are not likely representative for the
120 entire catchment. An increasing need for spatially distributed estimation of DDF_s has been
121 identified (Hock, 1999; Nester *et al.*, 2011). However, only few studies have attempted to
122 develop temperature-index methods in a distributed manner (Cazorzi and DallaFontana, 1996;
123 Williams and Tarboton, 1999; Daly *et al.*, 2000 etc.). Most of them computed the DDF_s as a
124 function of a radiation index, snow albedo, rainfall rate, elevation, snow density or wind
125 speed, which are heavily affected by topography, thus addressing the spatial variability of
126 snowmelt in mountain terrain (Dunn and Colohan, 1999; Hock, 2003). However, due to the
127 complex interactions between atmospheric and surface characteristics affecting the

128 degree-day factor, the relationship between DDF_s and these characteristics is still not very
129 well understood.

130 The objective of this study is to propose a new method for estimating spatial patterns of
131 DDF_s from MODIS data in mountain catchments. In comparison to traditional methods, the
132 DDF_s is not calibrated to observed runoff and snow water equivalent data, but directly
133 estimated from MODIS snow covered area and snow depth data alone. Snow depths can be
134 more widely measured in the field than snow water equivalent. For example, Environment
135 Canada gauges snow depth at 1556 sites, but snow water equivalent only at 27 sites. Similarly,
136 the U.S. Weather Service and the Swiss Service measure many more depths than water
137 equivalents (Johnson and Schaefer, 2002; Zhou *et al.*, 2005; Sturm *et al.*, 2010). The new
138 proposed method differs from existing estimation methods of DDF_s in a number of ways:
139 First, snow water equivalent is estimated from MODIS snow cover, snow depths and
140 precipitation data, so there is no need for snow water equivalent measurements which are
141 difficult to obtain in most mountain watersheds. Second, DDF_s is estimated on a
142 subcatchment scale rather than on a point scale as in most traditional estimation methods.
143 Third, the study extends the idea of partitioning hydrological time series to explore hidden
144 hydrological information of He *et al.* (2014) to the case of snow data. The methodology is
145 tested in a mountain basin in Austria.

146 The remainder of this paper is organized in the following way: Section 2 details the
147 estimation method of spatial snow density and the snowmelt degree-day factor, as well as the
148 stepwise calibration method for the model parameters. Section 3 contains a description of the
149 geographic and hydrological characteristics of the study basin, including the main data
150 sources and data preprocessing. Section 4 presents the main simulation results and
151 comparisons between the hydrologic model performance using DDF_s estimated from snow
152 data and DDF_s calibrated on runoff. Finally, section 5 provides a summary of the study, and
153 discusses possible sources of uncertainty in the results and further applications of the new
154 estimation methods of degree-day factors.

155 **2 Methodology**

156 The main idea of estimating the degree-day factor is as follows. The volume of snow for
157 each subcatchment and each day is estimated using MODIS SCA data and ground-based snow

158 depth time series. The snow volume time series are partitioned in time into three groups,
 159 based on the daily air temperatures: days with snow accumulation (when temperatures are
 160 below a threshold), days with ablation (when temperatures are above a different threshold)
 161 and days where both processes occur (when temperatures are between the thresholds). Snow
 162 density is estimated from the days with snow accumulation as the ratio between measured
 163 precipitation and changes in snow volume. The degree-day factor is estimated from the days
 164 with ablation as the ratio between measured changes in snow water equivalent (product of
 165 snow volume and density) and the difference between daily temperature and the threshold
 166 value.

167 For comparison, DDF_s is calibrated on runoff using a semi-distributed hydrological
 168 model--THREW which has been applied in several studies (Tian *et al.*, 2006,2008,2012; Mou
 169 *et al.*, 2008; Li *et al.*, 2012). The calibration follows the stepwise procedure developed by He
 170 *et al.* (2014) but was slightly modified because of the local characteristic of the study basin
 171 (see Section 2.2). The study basin is divided into 95 subcatchments for the simulations.

172 The estimated degree-day factors are tested by simulations of basin runoff and snow
 173 cover patterns. The study period for which the analyses are performed is ten years, 2001-2010.
 174 2001 to 2005 is the calibration period and 2006 to 2010 is the validation period.

175 2.1 Estimation of degree-day factor from snow data

176 The observed snow data used to estimate the degree-day factor, DDF_s, are snow covered
 177 area (SCA) products and ground-based snow depths. Firstly, we obtain the volume per area of
 178 snow in each subcatchment and for each day by $V_s = \text{SCA} \cdot D_s$, where D_s is the average snow
 179 depth. Since the average snow depths tend to overestimate the snow covered area, therefore
 180 the multiplication with SCA is needed to compensate for the biases. In a next step, the change
 181 of snow water equivalent (SWE) between two days, $\frac{dSWE}{dt} = \rho_s \cdot \frac{dV_s}{dt}$, is attributed to three
 182 snow processes according to Eq. (1a-c).

$$183 \quad \rho_s \cdot \frac{dV_s}{dt} = \begin{cases} P, & \text{for } T < T_S & \text{Accumulation (1a)} \\ P_s - M, & \text{for } T_S \leq T \leq T_R & \text{Combination (1b)} \\ -DDF \cdot (T - T_m), & \text{for } T > T_R & \text{Ablation (1c)} \end{cases}$$

184 where, ρ_s is the snow density, P is daily precipitation, P_s is daily snowfall, M is daily
 185 snowmelt depth, T_S is the temperature threshold below which all precipitation is in the form of

186 snowfall, T_R is the temperature threshold above which all precipitation is liquid, and T_m is the
 187 temperature threshold controlling the occurrence of melt. T_m usually falls between T_S and T_R .
 188 Rainfall and snowfall in the temperature window between T_S and T_R are simply estimated as
 189 half of the total precipitation. The value of the three temperature thresholds are set as $T_m = T_S =$
 190 0.0°C and $T_R = 2.5^\circ\text{C}$ in this study following Parajka *et al.* (2007). The V_s time series are
 191 partitioned into three segments, i.e. accumulative segment, a combination segment and an
 192 ablative segment according to Eq. 1a-c.

193 The snow density (ρ_s) is calculated from the days with accumulation based on the
 194 observed V_s and P according to Eq. 1a. As the snow cover volume can still change after
 195 snowfall events due to gravity and condensation, snowfall events that produce a stable snow
 196 cover volume are selected for the estimation of snow density. Therefore, snowfall events in
 197 the accumulative segment that ended by at least three no-snowfall days, and where the
 198 relative difference of the V_s value between the last three no-snowfall days is lower than 10%,
 199 are selected for the calculation of snow density. In these events, the cumulative snowfall (ΔP_s)
 200 is the sum of the daily precipitation values, and the change of snow cover volume (ΔV_s^*) is the
 201 difference of the V_s values between the last no-snowfall day and the first snowfall day. Snow
 202 density in each event is obtained as $\rho_s = \Delta P_s / \Delta V_s^*$. This calculation is carried out for each
 203 subcatchment. A representative value of the density for each subcatchment is estimated as the
 204 average of all event values, neglecting any changes of density during snow melt. While this is
 205 a simplification, it should be noted that the melt period is often interrupted by accumulation
 206 events, thus the differences between accumulation and ablation densities are not considered to
 207 be very large.

208 The snowmelt degree-day factor DDF_s is calculated from days with ablation based on
 209 changes in the snow water equivalent and air temperatures according to Eq. 1c. The change of
 210 snow water equivalent between days is calculated as $\Delta V_s \cdot \rho_s$, where the density ρ_s estimated
 211 above is used. The degree-day temperature is calculated as the difference between the daily
 212 temperature (T) and the threshold value (T_m). Daily DDF_s value are then estimated as
 213 $\text{DDF}_s = \frac{dV_s}{dt} \cdot \frac{\rho_s}{T - T_m}$. Again, a representative value of the degree-day factor for each
 214 subcatchment is estimated as the average of all event values. Both the estimations of snow

215 density and DDF_s are carried out in the two sub-periods (2001-2005 and 2006 to 2010)
216 separately.

217 **2.2 Calibration of degree-day factor on runoff by a hydrologic model**

218 The runoff generation processes simulated by the THREW model includes subsurface
219 baseflow, rainfall runoff, snowmelt and glacier melt. Rainfall runoff is simulated by a
220 Xin'anjiang module, which adopts a water storage capacity curve to describe the non-uniform
221 distribution of water storage capacity in a subcatchment (Zhao, 1992). The storage capacity
222 curve is determined by two parameters (spatial averaged storage capacity WM and shape
223 coefficient B). Rainfall runoff is generated on areas where the storage capacity is reached.
224 The remainder of the rainfall infiltrates into the soil and becomes an additional contribution to
225 subsurface baseflow which is calculated by two outflow coefficients (KKA and KKD). Snow
226 and glacier melt are simulated by a degree-day model with different degree-day factors
227 (DDF_s and DDF_G , respectively). Precipitation in the snow covered areas is divided into
228 rainfall and snowfall according to two threshold temperature values (0°C and 2.5°C are
229 adopted in this study). Between the two thresholds, mixed snow and rain is assumed to occur.
230 Snow water equivalent in each subcatchment is updated daily with snowfall and snowmelt,
231 while the glacier area is assumed to be stable during the study period. The model parameters
232 are grouped according to the runoff generation mechanisms, i.e., a subsurface baseflow group
233 (KKA and KKD), a snowmelt group (DDF_s), a glacier melt group (DDF_G) and a group where
234 rainfall directly becomes runoff (WM and B) (see He *et al.* (2014)). Each parameter group is
235 calibrated separately in a stepwise way by manual calibration. The stepwise calibration is
236 similar to that proposed by He *et al.* (2014). In a first step, the hydrograph is partitioned
237 according to three indices, S_i , G_i , D_i , which are defined as 0 or 1 (Eq. (2)-(4)) according to the
238 water source for runoff generation on each day (subsurface baseflow, snowmelt, glacier melt
239 and rainfall). Next, each parameter group is related to an individual hydrograph partition and
240 calibrated on the corresponding partition separately.

$$S_i = \begin{cases} 1, & \text{if } \max_{j=1 \rightarrow 95} (T_j) \geq T_m \\ 0, & \text{otherwise} \end{cases} \quad \text{Snowmelt} \quad (2)$$

$$241 \quad G_i = \begin{cases} 1, & \text{if } \max_{j=1 \rightarrow n} (T'_j) \geq T_m \\ 0, & \text{otherwise} \end{cases} \quad \text{Glacier melt} \quad (3)$$

$$D_i = \begin{cases} 1, & \text{if } \max_{j=1 \rightarrow 95} (T_j) \geq T_s \wedge \sum_{j=1 \rightarrow 95} P_j \geq 0 \\ 0, & \text{otherwise} \end{cases} \quad \text{Rainfall runoff} \quad (4)$$

242 where, i is the day index, S_i , G_i and D_i are the indices indicating the occurrence of snowmelt,
 243 glacier melt and rainfall runoff, respectively. Values equal to 1 indicate that snowmelt, glacier
 244 melt and rainfall runoff, respectively, can be a water source for runoff generation on that day.
 245 Values equal to 0 indicate that this is not the case. T_j is the daily temperature in the
 246 subcatchment j , T'_j is the daily temperature in the glacier covered part of subcatchment j , n is
 247 the number of subcatchment that are covered with glacier, and P_j is the daily precipitation in
 248 subcatchment j . Based on the daily values of the three indices, the daily hydrograph is
 249 segmented into four partitions in Eq. (5):

$$250 \quad Q = \begin{cases} Q_{SB}, & \text{for } S_i + G_i + D_i = 0 \\ Q_{SB} + Q_{SM}, & \text{for } S_i - G_i - D_i = 1 \\ Q_{SB} + Q_{SM} + Q_{GM}, & \text{for } G_i - D_i = 1 \\ Q_{SB} + Q_{SM} + Q_{GM} + Q_R, & \text{for } D_i = 1 \end{cases} \quad (5)$$

251 where, Q_{SB} stands for the subsurface baseflow. It dominates the basin hydrograph when both
 252 melt water and rainfall runoff do not occur ($S_i + G_i + D_i = 0$). Q_{SM} represents snowmelt, Q_{GM}
 253 represents glacier melt water and Q_R represents the direct rainfall runoff. The partition is
 254 based on the assumption that the convergence time of drainage in the basin is no longer than
 255 one day.

256 The parameter groups are calibrated on different partitions in a stepwise way: The
 257 parameter group controlling subsurface baseflow is first calibrated on the Q_{SB} partition. Then,
 258 the degree-day factors for snowmelt and glacier melt are calibrated on the $Q_{SB} + Q_{SM}$ and
 259 $Q_{SB} + Q_{SM} + Q_{GM}$ partitions separately. Parameters for rainfall runoff are calibrated on the
 260 $Q_{SB} + Q_{SM} + Q_{GM} + Q_R$ partition in a last step. We use $\log RMSE$ as the goodness of fit measure
 261 for the calibration of subsurface baseflow and $RMSE$ for the calibration of degree-day factors
 262 and rainfall runoff parameters. Finally, we combine the simulations of each partition to obtain

263 the entire daily simulation of basin discharge and evaluate it using NSE , $\log NSE$, VE and a
 264 combined performance measure ME (Eq. (6)-(9)).

$$NSE = 1 - \frac{\sum_{i=1}^n (Q_{obs}(i) - Q_{sim}(i))^2}{\sum_{i=1}^n (Q_{obs}(i) - \bar{Q}_{obs}(i))^2} \quad (6)$$

$$\log NSE = 1 - \frac{\sum_{i=1}^n (\log Q_{obs}(i) - \log Q_{sim}(i))^2}{\sum_{i=1}^n (\log Q_{obs}(i) - \log \bar{Q}_{obs}(i))^2} \quad (7)$$

265

$$VE = 1 - \frac{\sum_{i=1}^n |Q_{obs}(i) - Q_{sim}(i)|}{\sum_{i=1}^n Q_{obs}(i)} \quad (8)$$

$$ME = NSE + \log NSE + VE \quad (9)$$

$$RMSE = \sqrt{\frac{1}{n} \sum_{i=1}^n (Q_{obs}(i) - Q_{sim}(i))^2} \quad (10)$$

266 2.3 Evaluation of estimated DDF_s from snow data

267 The estimated values of DDF_s are evaluated in the study period by applying their value
 268 in the THREW hydrological model and comparing the new simulations of runoff and snow
 269 cover patterns with those obtained by DDF_s calibrated on runoff. The evaluation is carried out
 270 in three basins with different catchment area, elevation and glacier melt contributions to the
 271 total runoff. The ME values of daily discharge simulation and $RMSE$ values of the simulation
 272 of the snowmelt dominated hydrograph partition ($Q_{SB} + Q_{SM}$) in the three basins are used to
 273 evaluate the performance of the runoff simulation. The fit between simulated and observed
 274 SCA series and spatial snow cover patterns by MODIS is used to assess the simulations of
 275 snow cover.

276 3 Data

277 3.1 Study area

278 The methodology is evaluated in the Lienz catchment which is located in East Tyrol,
 279 Austria, and covers an area of 1198 km². Its elevations range from 670 m a.s.l. to 3775 m
 280 a.s.l., and approximately 7% of the region is covered by glacier (Fig. 1). Its annual mean
 281 temperature is approximately 1.7 °C, and annual mean precipitation is about 1164 mm.
 282 Snowmelt water is an important water source for local runoff generation, especially in the
 283 spring season when approximately 70% of the basin is covered by snow (Blöschl *et al.*, 1990).

284 The topographic feature of the basin is depicted by a 25 m resolution Digital Elevation Model
285 which is used to divide the study basins into subcatchment units. The three basins (Lienz,
286 Waier and Innerschloess, see Fig. 1) in the study area are further divided into 95
287 subcatchments, 29 subcatchments and 9 subcatchments respectively for the hydrological
288 modeling. The runoff concentration time can be considered as approximately one day in this
289 catchment (Blöschl *et al.*, 1990).

290 **3.2 Snow data**

291 The MODIS snow covered area (SCA) data used in this study is the daily product, i.e.
292 MOD10A1 and MYD10A1 (V005) (Hall *et al.*, 2006 a, b). It has been downloaded from the
293 website of the National Snow and Ice Data Center (NSIDC, www.nsidc.org). The used data
294 set has a spatial resolution of 500 m and consists of daily snow cover maps from 1 January
295 2001 to 31 December 2010. The original Terra and Aqua products were merged in space and
296 time to reduce cloud coverage by Parajka and Blöschl (2008b). Only the MODIS SCA data
297 for those days when the cloud coverage of the basin was less than 50% after the merging
298 procedure are used. To obtain a continuous time series of SCA, we implemented a linear
299 interpolation between two valid SCA values.

300 Snow depth data observed at 1091 stations in Austria (7 stations in the study area) are
301 spatially interpolated by external drift kriging based on elevation. The resulting data product
302 has a spatial resolution of 1 km. Snow depth in each subcatchment is the average value of all
303 the 1×1 km pixels inside.

304 **3.3 Hydrologic model inputs**

305 The daily precipitation data are spatially interpolated by external drift kriging from 1091
306 stations in Austria (7 stations in the study area). The temperature data are interpolated by the
307 least-squares trend prediction method from 221 stations in Austria (6 stations in the study
308 area). Both methods using elevation as an auxiliary variable (see Parajka *et al.* (2005)). Daily
309 streamflow data from three hydrological stations are used, Lienz, Waier and Innerschloess,
310 which drain areas of 1198 km², 285 km² and 39 km² respectively (see Fig. 1). The datasets
311 used in this study consist of two sub-periods, the first is a calibration period from January 1,
312 2001 to December 31, 2005 and the second is a validation period from January 1, 2006 to
313 December 31, 2010.

314 4 Results

315 4.1 Snow density and DDF_s

316 Based on Eq. (1a) and (1c), we obtained the snow densities and snowmelt degree-day
317 factors (DDF_s) for each subcatchment in the Lienz basin. For example, Figs 2 and 3 show the
318 spatial distribution of the snow density and DDF_s estimated in the calibration period. Figure 2
319 indicates that subcatchments in upstream have higher snow density and DDF_s values than that
320 in downstream. Figure 3 represents the relationships between snow density and elevation, and
321 DDF_s and elevation. Leaf area index (LAI) data from MODIS land cover products are used to
322 describe the vegetation coverage in each subcatchment in Fig. 3. Each dot stands for a
323 subcatchment, and its size reflects the annual mean LAI over the study period of the
324 corresponding subcatchment. The estimated values of snow density range from approximately
325 0.1 to 0.6 g/cm³ with a mean value of 0.3 g/cm³. The estimated values of DDF_s range from
326 about 1.6 to 4.5 mm/d/°C with an average of 2.7 mm/d/°C. DDF_s values in the medium sized
327 Waier basin mainly fall into a range of 2.0-3.0 mm/d/°C, while in the smallest basin, the
328 Innergschloess, they fall into a range of 2.0-4.0 mm/d/°C (see Fig. 2). Generally, both the
329 snow density and DDF_s values increase with increasing elevation (see Fig. 3), as would be
330 expected. The value of snow density can be affected by the duration of the snow cover. In
331 high elevation subcatchments, temperatures tend to be lower which leads to more snowfall
332 and more opportunity for compaction and settling which, in turn, tends to result in higher
333 snow densities (Rango and Martinec, 1995). The spatial pattern of DDF_s can be attributed to
334 the interaction of climate and basin topography as well as vegetation: At higher elevations,
335 soils tend to be thin and air temperatures tend to be low, which are unfavorable conditions for
336 the growth of vegetation. Therefore, the share of latent heat of transpiration in the energy
337 balance is lower. Lower temperatures at higher elevation also reduce the share of sensible
338 heat (Musselman *et al.*, 2012). Coupling with a stronger solar radiation due to lower
339 cloudiness, stronger snowmelt is produced at higher elevations relative to the difference
340 between daily temperature (T) and the threshold value (T_m). Higher elevations are also
341 associated with steep terrain which reinforces the melt rate by increasing the solar incident
342 angle on the south facing slopes (Blöschl *et al.*, 1991a,b; Blöschl and Kirnbauer, 1992). At
343 lower elevations, climate conditions are favorable for the growth of vegetation, which

344 produce a higher share of latent heat by transpiration and restrain the snowmelt. On the other
345 hand, higher vegetation canopies may contribute to higher soil water contents which may
346 increase the albedo of the land surface and may reduce the energy available for snowmelt
347 (Kuusisto, 1980). The moist soil can also enhance the temperature gradient and create sharp
348 gradients in sensible heat fluxes (Entekhabi *et al.*, 1996) and allow fast redistribution of soil
349 moisture at small scales (Western *et al.*, 1998). Changes of the heat conditions in the near
350 surface atmosphere in turn may change the soil moisture state and may promote vegetation
351 growth. The spatial variability of snow density and DDF_s is likely the combined result of a
352 number of factors, including slope aspect, wind speed and shading, in addition to elevation
353 and vegetation.

354 **4.2 Transferability in time of the estimated DDF_s**

355 The data set used in this study has been divided into two sub-periods: calibration period
356 from 1 January 2001 to 31 December 2005 and validation period from 1 January 2006 to 31
357 December 2010. The average annual precipitation is 1126 mm in the calibration period, and
358 1238 mm in the validation period. The mean daily temperature is 2.28°C in the calibration
359 period, and 2.59°C in the validation period. Mean daily snow coverage from MODIS is
360 approximately 10% in the calibration period, and about 12% in the validation period.
361 Although the difference of the climate and snow cover conditions in the two periods is small,
362 it can still play a role in the snowmelt processes. Therefore, we re-estimated the value of
363 snow density and DDF_s using the climate data and MODIS snow data in the validation period
364 and compared the new estimated DDF_s set with that estimated using data in the calibration
365 period in Fig. 4. The comparison shows that the two estimated sets of DDF_s and snow density
366 (SD) are slight different due to the different climate and snow cover conditions in the two
367 sub-periods. However, the correlation coefficients between the two estimated DDF_s sets and
368 that between the two SD sets are both high, i.e. 0.802 for the DDF_s and 0.720 for the SD (see
369 Fig. 4), which indicates that both the two estimated DDF_s sets and two SD sets are consistent
370 in the two sub-periods. There is no significant systematic bias for the estimated DDF_s and SD.
371 This suggests the transferability in time of the estimated DDF_s in the whole study period. To
372 further test its transferability in time, we applied DDF_s values estimated in one period for the
373 simulation of basin discharge and snow cover in the other period. For example, in the

374 following Section 4.4, we used the DDF_S set estimated by snow data in the calibration period
375 (2001 to 2005) for the model simulation in the validation period (2006 to 2010).

376 **4.3 Stepwise calibration**

377 Model parameters in the three basins are calibrated on the corresponding hydrograph
378 partitions separately (see He *et al.* (2014)). After the calibration, we combined the simulations
379 of the four partitions and obtained the entire simulation of daily discharge. As an example, the
380 simulation in each step in the largest basin, the Lienz basin, is shown in Fig. 5, using the
381 calibrated degree-day factors for snowmelt and glacier melt as $2.6\text{mm/d/}^\circ\text{C}$ and $3.5\text{mm/d/}^\circ\text{C}$
382 respectively, as shown in Table 1. The $\log RMSE$ and $RMSE$ values in Fig. 5 suggest that the
383 simulations of each hydrograph partition are very reasonable. The calibrated parameter set
384 was also tested for the validation period (2006-2010), as shown in Fig. 6. Again, the
385 performance is very reasonable as indicated by NSE and $\log NSE$. For example, in the Lienz
386 basin NSE values are 0.817 and 0.833 in the calibration and validation periods, respectively,
387 indicating the suitability of the calibrated parameter set. The simulation performances for the
388 two sub-basins (Waier and Innerschloess) are also shown in Table 1.

389 The calibrated DDF_S and DDF_G are slight different in the three basins. DDF_S ranges
390 from 1.0 to $2.6\text{mm/d/}^\circ\text{C}$, and DDF_G ranges from 3.5 to $6.0\text{mm/d/}^\circ\text{C}$. The calibrated DDF_S in
391 the Lienz and Waier basins are similar to those estimated from MODIS and snow depth data
392 in Sect. 4.1, while the calibrated value, $1.0\text{mm/d/}^\circ\text{C}$, in the Innerschloess basin is clearly
393 different from the estimated values that range from 2.0 to $4.0\text{mm/d/}^\circ\text{C}$. Given the role of
394 radiation in this high elevation basin, the value of $1.0\text{mm/d/}^\circ\text{C}$ seems far too low, and the
395 snow data based estimate is much more reasonable.

396 The runoff simulations in the medium basin (Waier) are the best with an NSE value of
397 0.832 in the calibration period and 0.863 in the validation period. Runoff simulations in the
398 smallest basin (Innerschloess) exhibit a slightly lower performance with an NSE value of
399 0.726 in the validation period. This may be partly due to the remarkably low value of the
400 calibrated DDF_S , i.e. $1.0\text{mm/d/}^\circ\text{C}$. The calibration of DDF_S relies heavily on the observed
401 hydrographs, which may introduce uncertainties in the DDF_S estimates in some cases.

402 **4.4 Evaluation of estimated DDF_S**

403 To evaluate the estimated DDF_S , we replaced the calibrated DDF_S in the model with the

404 ones estimated from snow data, and reran the hydrological simulation. The other model
 405 parameters remained the same as those calibrated in Sect. 4.3. The new simulation results in
 406 the three basins are summarized in Table 1. The simulations using the spatially variable DDF_s
 407 estimated from snow data tend to perform better than those using the calibrated, spatially
 408 uniform DDF_s . In the Lienz and Waier basins, the new simulations are similar to those shown
 409 in Sect. 4.3, as demonstrated by the ME values in Table 1. For example, Fig. 7 presents the
 410 new simulation for the Lienz basin with an NSE value of 0.810 in the calibration period and
 411 0.826 in the validation period. Both are very similar to the NSE values shown in Fig. 6. The
 412 mean value of the estimated DDF_s in these two basins are $2.7\text{mm/d/}^\circ\text{C}$ and $2.6\text{mm/d/}^\circ\text{C}$
 413 respectively, both are similar to the calibrated value of $2.6\text{mm/d/}^\circ\text{C}$. It is worth noting that the
 414 new simulation in the smallest Innergschloess basin is significantly better, especially in the
 415 validation period, considering the ME values in Table 1. The mean value of the estimated
 416 DDF_s in this basin is $3.2\text{mm/d/}^\circ\text{C}$ which is clearly different from the calibrated value. This
 417 suggests that the calibrated DDF_s value of $1.0\text{mm/d/}^\circ\text{C}$ in this small, high elevation basin
 418 may not be accurate.

419 As the DDF_s value has the most sensitive effect on the snowmelt dominated hydrograph
 420 partition ($Q_{SB}+Q_{SM}$), we focus on the simulation of this partition by the two DDF_s sets in Fig.
 421 8. The simulation performance is evaluated using $RMSE$. The first two rows in Fig. 8 show
 422 the simulations using calibrated (Fig. 8a-c) and estimated (Fig. 8d-f) DDF_s in the calibration
 423 period, and the last two rows present the simulations in the validation period (Fig. 8g-i is for
 424 DDF_s calibrated on runoff and Fig. 8j-l is for DDF_s estimated from snow data). The
 425 differences of the $RMSE$ values obtained by the two DDF_s sets in the Lienz basin (first
 426 column) range from 0.132 to 0.347 m^3s . Considering the relatively higher levels of the
 427 discharge, the two simulations can still be regarded as very close. As to the Waier basin
 428 (second column), the $RMSE$ value obtained by the estimated DDF_s in the calibration period is
 429 slightly higher (0.04 m^3s higher) but much lower (0.263 m^3s lower) in the validation period.
 430 In Innergschloess basin (third column), the $RMSE$ values in the calibration period are as close
 431 as a slight difference of 0.016 m^3s , while in the validation period the $RMSE$ value obtained
 432 by the estimated DDF_s is 0.118 m^3s lower than that obtained by the calibrated DDF_s .
 433 Comparisons of the simulations of the $Q_{SB}+Q_{SM}$ hydrograph partition show a similar

434 performance in the calibration period but a better performance of estimated DDF_s in the
435 validation period. Overall, the comparisons for the three basins shown in Table 1 and Fig. 8
436 suggest that the DDF_s values estimated from snow data by the new method tend to produce a
437 somewhat better runoff simulation performance.

438 We also assess the suitability of the estimated DDF_s values by examining the snow cover
439 simulations in the study basins. The match between simulated snow cover and observed snow
440 cover from MODIS is illustrated in Fig. 9 to Fig.12. The THREW model simulates snow
441 water equivalent (SWE) in each subcatchment. To obtain the snow covered area (SCA) in the
442 basin, we define a threshold value for the simulated SWE (SWE_T), above which the sub unit
443 of the basin (i.e. subcatchment) is considered to be fully covered by snow, and below it the
444 subcatchment is considered snow free. Subsequently, we obtain the simulated time series of
445 SCA of the study basin. For example, Fig. 9 shows the comparison of simulated SCA using
446 DDF_s calibrated on runoff and DDF_s estimated from snow data, and the observed SCA from
447 MODIS in both calibration and validation periods in the Lienz basin. Fig. 10 shows a similar
448 figure for Innergschloess. The black dots in Figs. 9 and 10 are the MODIS observed SCA
449 values on days when the observed cloud coverage in the basin was lower than 20%. The
450 similarity of the simulated SCA and observed SCA (just for the days when MODIS was
451 available) is evaluated using $RMSE$, where $RMSE_c$ relates to the simulations using calibrated
452 DDF_s and $RMSE_e$ relates to the simulations using estimated DDF_s . We determine the SWE_T
453 threshold by optimizing the $RMSE_c$ values in the calibration period in the Lienz basin which
454 resulted in a value of 18 mm. Parajka and Blöschl (2008a) give details on how the threshold
455 can be chosen.

456 Generally, the simulated snow covered areas by the two DDF_s sets are similar and both
457 are close to those observed by MODIS in the Lienz basin. The similarity can be attributed to
458 the similar value of estimated and calibrated DDF_s in this basin. It is interesting that the
459 simulation of SCA by estimated DDF_s (green lines) still has a higher performance as
460 indicated by the lower $RMSE_e$ values in both calibration and validation periods. As to the
461 simulation in Innergschloess shown in Fig. 10, the simulated SCA using estimated DDF_s
462 (green lines) matches the MODIS observed SCA significantly better than that simulated by
463 calibrated DDF_s (red lines) in both calibration and validation periods. The $RMSE_e$ values are

464 approximately 0.07 lower than the $RMSE_c$ values (Fig. 10). This result suggests that the
465 DDF_s values estimated from snow data in this basin represent the snowmelt pattern better
466 than the value calibrated on runoff.

467 Several days with available MODIS data (black dots in Fig. 9) were selected to analyze
468 the snow patterns in Figs. 11-12. The selected days include April 29th, May 7th and June 10th
469 in 2003, and April 27th, May 7th and May 27th in 2008. The snow patterns are expressed as the
470 spatial distribution of simulated SWE using calibrated DDF_s and estimated DDF_s , and the
471 spatial distribution of SCA observed by MODIS. Figs. 11 and 12 show the results for the
472 calibration period and validation period, respectively. Sub-catchments are covered with snow
473 refers to purple surfaces in Figs. 11 and 12. The intensity of the purple color increases with
474 the increasing of the value of snow coverage (SCA) from MODIS or simulated SWE. The
475 green surface in the two figures refers to areas where SCA value from MODIS or the
476 simulated SWE value is zero, i.e. non-snow covered areas. Generally, a higher simulated
477 SWE value corresponds to a higher MODIS SCA value in that subcatchment. All the three
478 snow patterns show a clear snow ablation process from late April to late May. In April, most
479 of the basin area is covered by snow, and the snow water equivalent can be as high as
480 600-700mm, while snow cover almost disappears in late May 2003. May is a snowmelt flood
481 month which is also indicated in Fig. 6 by the abrupt increase of discharge in this month.
482 However, there are some differences between the three snow patterns. In the upstream
483 subcatchments the simulated snow water equivalent using calibrated DDF_s is higher than that
484 using estimated DDF_s . Correspondingly, the simulated sub-catchments are covered with snow
485 using calibrated DDF_s are more than those observed from MODIS (see Figs. 11 and 12 on
486 June 10th, 2003 and May 27th, 2008). In the downstream subcatchments, simulated snow
487 covered sub-catchments by the two DDF_s sets are both less than the observed ones (see Figs.
488 11 and 12 on April 29th, 2003 and May 7th, 2008). Overall, the similarity between the spatial
489 distribution of snow covered sub-catchments simulated using estimated DDF_s and the spatial
490 distribution observed by MODIS is higher than that simulated using calibrated DDF_s , which
491 can be seen for May 7th, June 10th in 2003, and April 27th and May 27th in 2008. MODIS data
492 were one of the inputs to estimating DDF_s , so this result shows the consistency and usefulness
493 of the estimates.

494 5 Discussion and conclusions

495 This study proposes a method for estimating snowmelt degree-day factor (DDF_s) based
496 on MODIS snow cover data and snow depth data. DDF_s is estimated in each subcatchment of
497 the study basin separately. The spatial distribution of DDF_s shows a strong correlation with
498 elevation. Subcatchments with high elevations are associated with higher DDF_s values, which
499 can be partly attributed to the interactions of climate conditions, topography and vegetation.
500 The comparisons between simulations using DDF_s estimated from snow data and DDF_s
501 calibrated on runoff in terms of discharge and snow cover patterns show that the estimated
502 DDF_s are indeed more plausible than the calibrated DDF_s. The better performance can be
503 attributed to two advantages of the estimation method: First, using spatially variable snow
504 cover data from MODIS and snow depth data, it is possible to estimate DDF_s in a spatially
505 distributed fashion, while the calibrated DDF_s are lumped values and therefore spatially
506 uniform. Second, the values of DDF_s are estimated directly from observed snow cover data,
507 accounting for snow density, without involving runoff processes. The direct estimation should
508 have a stronger physical basis than the calibration in which the value of DDF_s is influenced
509 by a number of hydrological processes and the interactions of hydrological model parameters
510 (Merz *et al.*, 2011). However, the modeling improvement when using the spatially distributed
511 DDF_s should indeed be different for different modeling scales. The modeling scale, i.e. size
512 of fundamental computational unit (sub-catchment in this study), can have a significant
513 influence on the simulation, considering the spatial resolution of MODIS data and the spatial
514 density of gauge stations for precipitation and temperature. Adopting different sub-catchment
515 sizes in the model could be a potential way to analyze the scale effect on the simulation,
516 which can be an issue for further study.

517 The estimated values of snow density and DDF_s are fully consistent with those estimated
518 by Kuusisto (1980), Rango and Martinec (1995), Parajka *et al.* (2005) and Sturm *et al.* (2010).
519 The values of snow density estimated in Sturm *et al.* (2010) in Canada and the United States
520 fell into a range of 0.19 to 0.51 g/cm³, and the DDF_s of snowmelt estimated in Parajka *et al.*
521 (2005) in Austria ranged from approximately 0.5 to 5.0 mm/d/°C. The simulations of snow
522 cover patterns show an obvious snow ablation process from late April to late May in the study
523 basin, which was also indicated by Blöschl *et al.* (1990). The performance of the runoff

524 simulations in this study is also very reasonable (*NSE* almost always >0.8). For example, the
525 runoff simulations of Parajka *et al.* (2007) in 320 catchments in Austria based on automatic
526 calibration gave *NSE* mean values of about 0.75 in calibration period and 0.70 in validation
527 period. Considering that high *NSE* values are relatively easier to be reached in snowmelt
528 affected basins, the performance of the stepwise calibration method should be evaluated in
529 further studies. It is believed that the actual model performance is similar to that of automatic
530 methods, yet the parameter estimates may be more plausible as different parameter groups are
531 estimated separately, which reduces the problem of parameter interdependence in the
532 calibration process.

533 It should be noted that the estimated values of snow density and DDF_S are associated
534 with a number of uncertainty sources: the temperature threshold values that determine the
535 occurrence of snowmelt (T_m) and the transition between liquid and solid precipitation (i.e. T_S
536 and T_R) and also the spatial interpolation method of the snow depth data. Usually, the value of
537 T_m falls in between the values of T_S and T_R in mountain basins. As long as the temperature is
538 higher than T_R , the change of snow water equivalent (SWE) can be attributed to snowmelt
539 alone. When the temperature is lower than T_S , basin snow water equivalent will be affected by
540 snowfall alone. The proposed estimation method can be used in mountain basins with variable
541 values of T_m , T_S and T_R in different basins. Reliable snow depth data are important for
542 estimating snow density and DDF_S well. To obtain the spatial distribution of snow depth,
543 measured data in 7 stations in the study area were interpolated here. The interpolation method
544 can play a significant role. Importantly, in this paper we made the assumption that snow
545 density during days of accumulation is similar to the density during days of ablation. This is
546 an assumption that needs further analysis on the basis of detailed snow data. Also the analysis
547 of the sensitivity of the results to other uncertainty sources could be the topic of future work.

548 **Acknowledgements**

549 This study was supported by the National Science Foundation of China (NSFC 51190092,
550 U1202232, 51222901) and the foundation of the State Key Laboratory of Hydroscience and
551 Engineering of Tsinghua University (2014-KY-01). We would like to thank the International
552 Communication Fellowship of Tsinghua University for financial support. We also thank
553 Thomas Nester and Jürgen Komma for their helpful suggestions on the hydrological modeling
554 in Austria, and Magdalena Rogger for providing the hydrogeology data in the study area.

555 **References**

- 556 Andreadis, K. M. and Lettenmaier, D. P.: Assimilating remotely sensed snow observations
557 into a macroscale hydrology model, *Adv. Water Resour.*, 29, 872-886, 2006.
- 558 Bach, H., Braun, M., Lampart, G. and Mauser, W.: Use of remote sensing for hydrological
559 parameterisation of Alpine catchments, *Hydrol. Earth Syst. Sci.*, 7, 862-876, 2003.
- 560 Blöschl, G., Gutknecht, D. and Kirnbauer, R.: Distributed snowmelt simulations in an Alpine
561 catchment.2. Parameter study and model predictions, *Water Resour. Res.*, 3181-3188,
562 1991b.
- 563 Blöschl, G. and Kirnbauer, R.: An analysis of snow cover patterns in a small Alpine
564 catchment, *Hydrol. Process.*, 6, 99-109, 1992.
- 565 Blöschl, G., Kirnbauer, R. and Gutknecht, D.: Distributed snowmelt simulations in an Alpine
566 catchment.1. model evaluation on the basis of snow cover patterns, *Water Resour. Res.*,
567 27, 3171-3179, 1991a.
- 568 Blöschl, G., Kirnbauer, R. and Gutknecht, D.: Modelling snowmelt in a mountainous river
569 basin on an event basis, *J. Hydrol.*, 113, 207-229, 1990.
- 570 Bormann, K. J., Evans, J. P. and McCabe, M. F.: Constraining snowmelt in a
571 temperature-index model using simulated snow, *J. Hydrol.*, Available online 11 June
572 2014, in press, doi: 10.1016/j.jhydrol.2014.05.073, 2014.
- 573 Bormann, K. J., Westra, S., Evans, J. P. and McCabe, M. F.: Spatial and temporal variability
574 in seasonal snow density, *J. Hydrol.*, 484, 63-73, 2013.
- 575 Cazorzi, F. and DallaFontana, G.: Snowmelt modelling by combining air temperature and a
576 distributed radiation index, *J. Hydrol.*, 181, 169-187, 1996.
- 577 Daly, S. F., Davis, R., Ochs, E. and Pangburn, T.: An approach to spatially distributed snow
578 modelling of the Sacramento and San Joaquin basins, California, *Hydrol. Process.*, 14,
579 3257-3271, 2000.
- 580 Dery, S. J., Salomonson, V. V., Stieglitz, M., Hall, D. K. and Appel, I.: An approach to using
581 snow areal depletion curves inferred from MODIS and its application to land surface
582 modelling in Alaska, *Hydrol. Process.*, 19, 2755-2774, 2005.
- 583 Dunn, S. M. and Colohan, R.: Developing the snow component of a distributed hydrological
584 model: a step-wise approach based on multi-objective analysis, *J. Hydrol.*, 223, 1-16,

585 1999.

586 Entekhabi, D., Rodriguez-Iturbe, I. and Castelli, F.: Mutual interaction of soil moisture state
587 and atmospheric processes, *J. Hydrol.*, 184, 3-17, 1996.

588 Fierz, C., Riber, P., Adams, E. E., Curran, A. R., Fohn, P., Lehning, M. and Pluss, C.:
589 Evaluation of snow-surface energy balance models in alpine terrain, *J. Hydrol.*, 282,
590 76-94, 2003.

591 Georgievsky, M. V.: Application of the Snowmelt Runoff model in the Kuban river basin
592 using MODIS satellite images, *Environ. Res. Lett.*, 4, doi:10.1088/1748-9326/4/4/0450,
593 2009.

594 Hall, D. K. and Riggs, G. A.: Accuracy assessment of the MODIS snow products, *Hydrol.*
595 *Process.*, 21, 1534-1547, 2007.

596 Hall, D. K., Riggs, G. A., Salomonson, V. V., DiGirolamo, N. E. and Bayr, K. J.: MODIS
597 snow-cover products, *Remote Sensing of Environment*, 83, 181-194, 2002.

598 Hall, D. K., Tait, A. B., Foster, J. L., Chang, A. and Allen, M.: Intercomparison of
599 satellite-derived snow-cover maps, *Annals of Glaciology* 31, 2000, 31, 369-376, 2000.

600 Hall, D. K., V. V. Salomonson, and G. A. Riggs. 2006a. MODIS/Terra Snow Cover Daily L3
601 Global 500m Grid. Version 5. Boulder, Colorado USA: National Snow and Ice Data
602 Center.

603 Hall, D. K., V. V. Salomonson, and G. A. Riggs. 2006b. MODIS/Aqua Snow Cover Daily L3
604 Global 500m Grid. Version 5. Boulder, Colorado USA: National Snow and Ice Data
605 Center.

606 Hamlet, F., Mote, W., Clark, P. and Lettenmaier, P.: Effects of Temperature and Precipitation
607 Variability on Snowpack Trends in the Western United States, *Journal of Climate*, 18,
608 4545-4561, 2005.

609 He, Z., Tian, F., Hu, H. C., Gupta, H. V. and Hu, H. P.: Diagnostic calibration of a
610 hydrological model in an alpine area, *Hydrol. Earth Syst. Sci. Discuss.*, 11, 1253-1300,
611 doi:10.5194/hessd-11-1253-2014, 2014, 2014.

612 Hinzman, L. D. and Kane, D. L.: Snow hydrology of a headwater arctic basin-2. conceptual
613 analysis and computer modeling, *Water Resour. Res.*, 27, 1111-1121, 1991.

614 Hock, R.: Temperature index melt modelling in mountain areas, *J. Hydrol.*, 282, 104-115,

615 2003.

616 Hock, R.: A distributed temperature-index ice- and snowmelt model including potential direct
617 solar radiation, *Journal of Glaciology*, 45, 101-111, 1999.

618 Howard, C.: Revisiting the degree-day method for snowmelt computations - Discussion,
619 *Water Resources Bulletin*, 32, 411-413, 1996.

620 Immerzeel, W. W., Droogers, P., de Jong, S. M. and Bierkens, M. F. P.: Large-scale
621 monitoring of snow cover and runoff simulation in Himalayan river basins using remote
622 sensing, *Remote Sensing of Environment*, 113, 40-49, 2009.

623 Jeelani, G., Feddema, J. J., van der Veen, C. J. and Stearns, L.: Role of snow and glacier melt
624 in controlling river hydrology in Liddar watershed (western Himalaya) under current and
625 future climate, *Water Resour. Res.*, 48, W12508, doi:10.1029/2011WR011590., 2012.

626 Johnson, J. B. and Schaefer, G. L.: The influence of thermal, hydrologic, and snow
627 deformation mechanisms on snow water equivalent pressure sensor accuracy, *Hydrol.*
628 *Process.*, 16, 3529-3542, 2002.

629 Kane, D. L., Gieck, R. E. and Hinzman, L. D.: Snowmelt modeling at small Alaskan arctic
630 watershed, *Journal of Hydrologic Engineering*, 2, 204-210, 1997.

631 Kirchner, J. W.: Getting the right answers for the right reasons: Linking measurements,
632 analyses, and models to advance the science of hydrology, *Water Resour. Res.*, 42,
633 W03S04, doi:10.1029/2005WR004362, 2006.

634 Klein, A. G. and Barnett, A. C.: Validation of daily MODIS snow cover maps of the Upper
635 Rio Grande River Basin for the 2000-2001 snow year, *Remote Sensing of Environment*,
636 86, 162-176, 2003.

637 Klok, E. J., Jasper, K., Roelofsma, K. P., Gurtz, J. and Badoux, A.: Distributed hydrological
638 modelling of a heavily glaciated Alpine river basin, *Hydrological Sciences Journal*, 46,
639 553-570, 2001.

640 Kuusisto, E.: On the values and variability of degree-day melting factor in Finland, *Nordic*
641 *Hydrology*, 11, 235-242, 1980.

642 Lang, H. and Braun, L.: On the information content of air temperature in the context of snow
643 melt estimation, In: Molnar, L., (Ed.), *Hydrology of Mountainous Areas*, Proceedings of
644 the Strbske Pleso Symposium 1990: IAHS Publ. no. 190, pp. 347-354, 1990.

645 Langston, G., Bentley, L. R., Hayashi, M., McClymont, A. and Pidlisecky, A.: Internal
646 structure and hydrological functions of an alpine proglacial moraine, *Hydrol. Process.*,
647 25, 2967-2982, 2011.

648 Lee, S. W., Klein, A. G. and Over, T. M.: A comparison of MODIS and NOHRSC
649 snow-cover products for simulating streamflow using the Snowmelt Runoff Model,
650 *Hydrol. Process.*, 19, 2951-2972, 2005.

651 Li, H. Y., Sivapalan, M. and Tian, F. Q.: Comparative diagnostic analysis of runoff
652 generation processes in Oklahoma DMIP2 basins: The Blue River and the Illinois River,
653 *J. Hydrol.*, 418, 90-109, 2012.

654 Li, X. G. and Williams, M. W.: Snowmelt runoff modelling in an arid mountain watershed,
655 Tarim Basin, China, *Hydrol. Process.*, 22, 3931-3940, 2008.

656 Liu, T., Willems, P., Feng, X. W., Li, Q., Huang, Y., Bao, A. M., Chen, X., Veroustraete, F.
657 and Dong, Q. H.: On the usefulness of remote sensing input data for spatially distributed
658 hydrological modelling: case of the Tarim River basin in China, *Hydrol. Process.*, 26,
659 335-344, 2012.

660 Luo, Y., Arnold, J., Liu, S. Y., Wang, X. Y. and Chen, X.: Inclusion of glacier processes for
661 distributed hydrological modeling at basin scale with application to a watershed in
662 Tianshan Mountains, northwest China, *J. Hydrol.*, 477, 72-85, 2013.

663 Martinec, J.: The degree-day factor for snowmelt-runoff forecasting, IAHS Publication, No.
664 51, *Surface Waters*, 468-477, 1960.

665 Maurer, E. P., Rhoads, J. D., Dubayah, R. O. and Lettenmaier, D. P.: Evaluation of the
666 snow-covered area data product from MODIS, *Hydrol. Process.*, 17, 59-71, 2003.

667 Marsh, C. B., Pomeroy, J. W. and Spiteri, R. J.: Implications of mountain shading on
668 calculating energy for snowmelt using unstructured triangular meshes, *Hydrol. Process.*,
669 26, 1767-1778, 2012.

670 Merz, R., Parajka, J. and Blöschl, G.: Time stability of catchment model parameters:
671 Implications for climate impact analyses. *Water Resources Research*, 47, W02531,
672 doi:10.1029/2010WR009505, 2011.

673 Mou, L., Tian, F., Hu, H. and Sivapalan, M.: Extension of the Representative Elementary
674 Watershed approach for cold regions: constitutive relationships and an application,

675 Hydrol. Earth Syst. Sci., 12, 565-585, 2008.

676 Musselman, K. N., Molotch, N. P., Margulis, S. A., Kirchner, P. B. and Bales, R. C.:
677 Influence of canopy structure and direct beam solar irradiance on snowmelt rates in a
678 mixed conifer forest, *Agricultural and Forest Meteorology*, 161, 46-56, 2012.

679 Nester, T., Kirnbauer, R., Gutknecht, D. and Blöschl, G.: Climate and catchment controls on
680 the performance of regional flood simulations, *J. Hydrol.*, 402, 340-356, 2011.

681 Ohmura, A.: Physical basis for the temperature-based melt-index method, *Journal of Applied*
682 *Meteorology*, 40, 753-761, 2001.

683 Parajka, J. and Blöschl, G.: The value of MODIS snow cover data in validating and
684 calibrating conceptual hydrologic models, *J. Hydrol.*, 358, 240-258, 2008a.

685 Parajka, J. and Blöschl, G.: Spatio-temporal combination of MODIS images - potential for
686 snow cover mapping, *Water Resour. Res.*, 44, 2008b.

687 Parajka, J., Merz, R. and Blöschl, G.: Uncertainty and multiple objective calibration in
688 regional water balance modelling: case study in 320 Austrian catchments, *Hydrol.*
689 *Process.*, 21, 435-446, 2007.

690 Parajka, J., Merz, R. and Blöschl, G.: A comparison of regionalisation methods for catchment
691 model parameters, *Hydrol. Earth Syst. Sci.*, 9, 157-171, 2005.

692 Parajka, J. and Blöschl, G.: MODIS-based Snow Cover Products, Validation, and Hydrologic
693 Applications. Chapter 9 in *Multi-scale Hydrological Remote Sensing: Perspectives and*
694 *Applications*, ed. By N.B. Chang and Y. Hong, CRC Press, Boca Raton, 185-212, 2012.

695 Rango, A. and Martinec, J.: Application of a snowmelt-runoff model using Landsat data,
696 *Nordic Hydrology*, 10, 225-238, 1979.

697 Rango, A. and Martinec, J.: Revisiting the degree-day method for snowmelt computations,
698 *Water Resources Bulletin*, 31, 657-669, 1995.

699 Singh, P. and Kumar, N.: Determination of snowmelt factor in the Himalayan region,
700 *Hydrological Sciences Journal*, 41, 301-310, 1996.

701 Singh, P., Kumar, N. and Arora, M.: Degree-day factors for snow and ice for Dokriani
702 Glacier, Garhwal Himalayas, *J. Hydrol.*, 235, 1-11, 2000.

703 Sturm, M., Taras, B., Liston, G. E., Derksen, C., Jonas, T. and Lea, J.: Estimating Snow
704 Water Equivalent Using Snow Depth Data and Climate Classes, *Journal of*

705 Hydrometeorology, 11, 1380-1394, 2010.

706 Tekeli, A. E., Akyurek, Z., Sorman, A. A., Sensoy, A. and Sorman, A. U.: Using MODIS
707 snow cover maps in modeling snowmelt runoff process in the eastern part of Turkey,
708 Remote Sensing of Environment, 97, 216-230, 2005.

709 Tian, F. Q., Hu, H. P. and Lei, Z. D.: Thermodynamic watershed hydrological model:
710 Constitutive relationship, Science in China Series E-Technological Sciences, 51,
711 1353-1369, 2008.

712 Tian, F. Q., Li, H. Y. and Sivapalan, M.: Model diagnostic analysis of seasonal switching of
713 runoff generation mechanisms in the Blue River basin, Oklahoma, J. Hydrol., 418,
714 136-149, 2012.

715 Tian, F., Hu, H., Lei, Z. and Sivapalan, M.: Extension of the Representative Elementary
716 Watershed approach for cold regions via explicit treatment of energy related processes,
717 Hydrol. Earth Syst. Sci., 10, 619-644, 2006.

718 Udnaes, H. C., Alfnes, E. and Andreassen, L. M.: Improving runoff modelling using
719 satellite-derived snow covered area? Nordic Hydrology, 38, 21-32, 2007.

720 Verbunt, M., Gurtz, J., Jasper, K., Lang, H., Warmerdam, P. and Zappa, M.: The hydrological
721 role of snow and glaciers in alpine river basins and their distributed modeling, J. Hydrol.,
722 282, 36-55, 2003.

723 Viviroli, D., Weingartner, R. and Messerli, B.: Assessing the hydrological significance of the
724 world's mountains, Mountain Research and Development, 23, 32-40, 2003.

725 Wang, X. W., Xie, H. J. and Liang, T. G.: Evaluation of MODIS snow cover and cloud mask
726 and its application in Northern Xinjiang, China, Remote Sensing of Environment, 112,
727 1497-1513, 2008.

728 Western, A. W., Blöschl, G. and Grayson, R. B.: How well do indicator variograms capture
729 the spatial connectivity of soil moisture? Hydrol. Process, 12, 1851-1868, 1998.

730 Williams, K. S. and Tarboton, D. G.: The ABC's of snowmelt: a topographically factorized
731 energy component snowmelt model, Hydrol. Process., 13, 1905-1920, 1999.

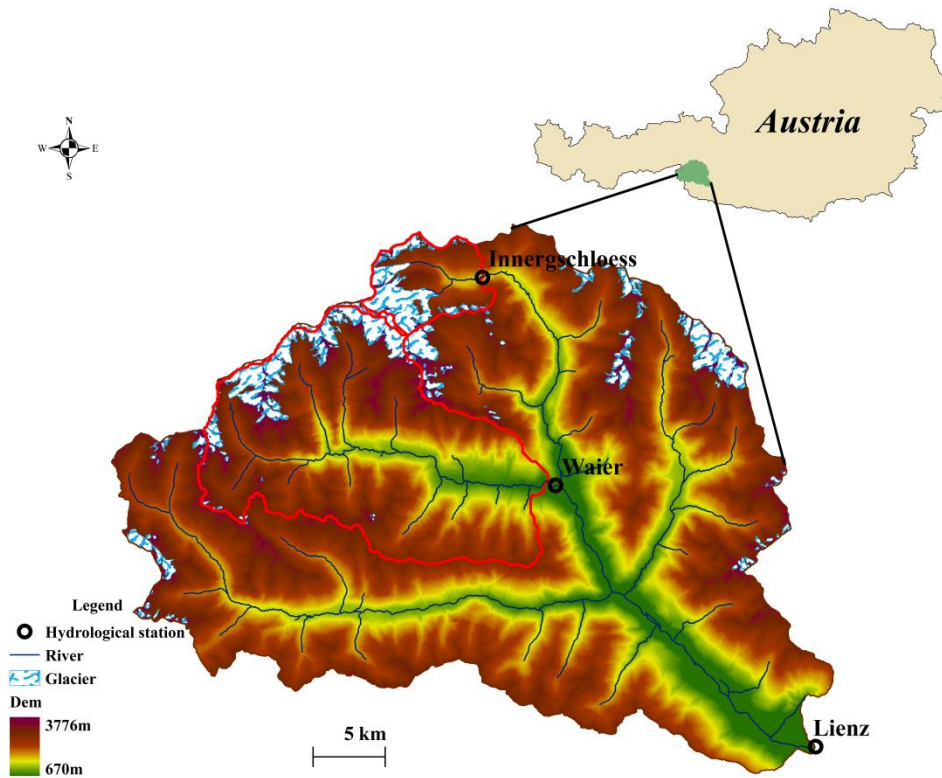
732 Zhang, S. Q., Gao, X., Ye, B. S., Zhang, X. W. and Hagemann, S.: A modified monthly
733 degree-day model for evaluating glacier runoff changes in China. Part II: application,
734 Hydrol. Process., 26, 1697-1706, 2012.

- 735 Zhao, R. J.: The Xin'anjiang model applied in China, *J. Hydrol*,135,371-381,1992.
- 736 Zhou, X. B., Xie, H. J. and Hendrickx, J.: Statistical evaluation of remotely sensed
737 snow-cover products with constraints from streamflow and SNOTEL measurements,
738 *Remote Sensing of Environment*, 94, 214-231, 2005.
- 739

740 Table 1. Performance of discharge simulations in three basins. DDF_S is the snowmelt degree-day factor
741 and DDF_G is the glacier melt degree-day factor. ME is the sum of NSE , $\log NSE$ and VE . The value of
742 DDF_S estimated from snow data is expressed as the spatial mean value +/- the mean difference of the
743 highest and the lowest value (in space) from the mean value. DDF_S values estimated by the proposed
744 method are shown in bold.

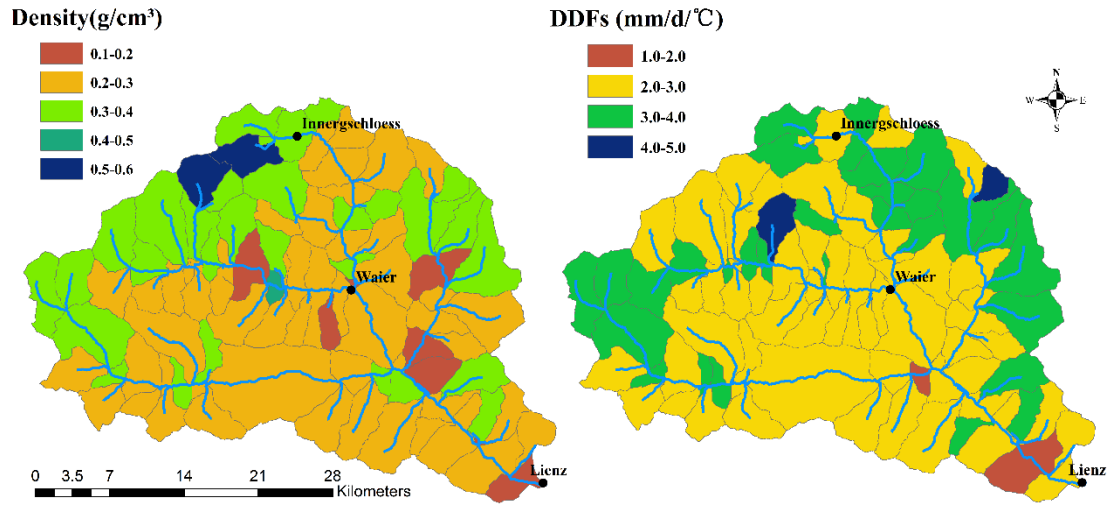
		Lienz		Waier		Innergshloess	
		Calibration	Validation	Calibration	Validation	Calibration	Validation
		Period	Period	Period	Period	Period	Period
DDF _S calibrated on runoff	DDF _S (mm/d/°C)	2.6	2.6	2.6	2.6	1.0	1.0
	DDF _G (mm/d/°C)	3.5	3.5	4.2	4.2	6.0	6.0
	<i>NSE</i>	0.817	0.833	0.832	0.863	0.804	0.726
	<i>logNSE</i>	0.851	0.873	0.849	0.871	0.825	0.871
	<i>VE</i>	0.762	0.758	0.739	0.770	0.654	0.585
	<i>ME</i>	2.430	2.464	2.420	2.504	2.283	2.182
DDF _S (mm/d/°C)		2.7 +/-1.1	2.7 +/-1.1	2.6 +/-0.9	2.6 +/-0.9	3.2 +/-0.3	3.2 +/-0.3
DDF _S estimated from snow data	DDF _G (mm/d/°C)	3.5	3.5	4.2	4.2	6.0	6.0
	<i>NSE</i>	0.810	0.826	0.835	0.845	0.801	0.768
	<i>logNSE</i>	0.845	0.867	0.845	0.869	0.826	0.885
	<i>VE</i>	0.751	0.746	0.740	0.760	0.648	0.628
	<i>ME</i>	2.406	2.439	2.420	2.474	2.275	2.281

745



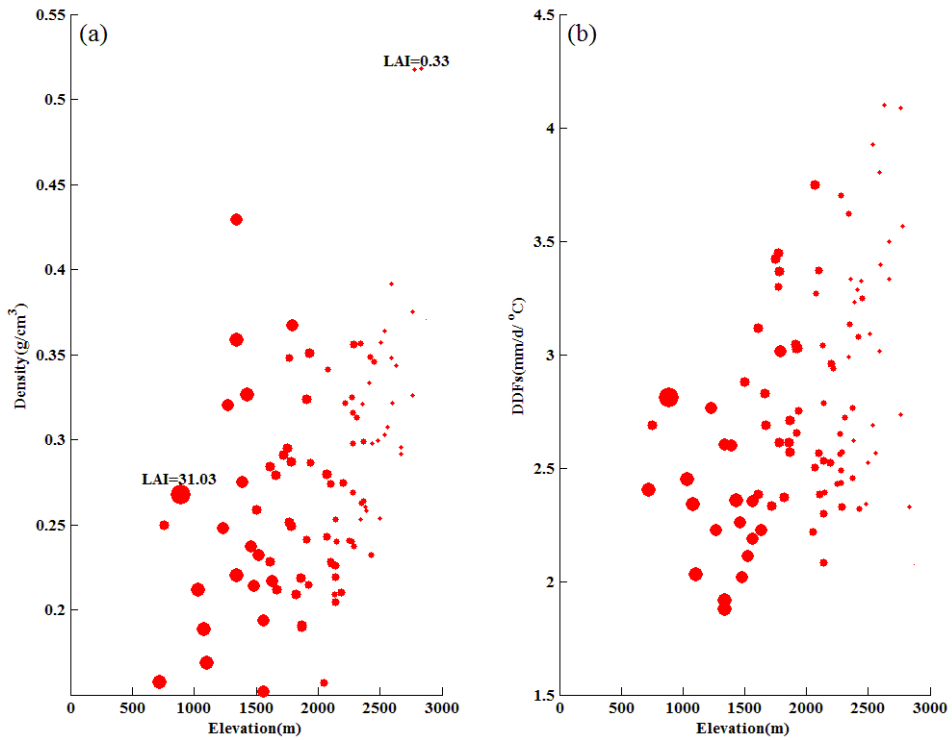
746
747
748
749

Figure 1. Location of the study area in Austria. Three catchments are analyzed, Lienz, Waier and Innerschloess, with areas of 1190 km², 285 km² and 39 km², respectively. The glacier coverage in the three basins is approximately 7%, 13% and 29%.



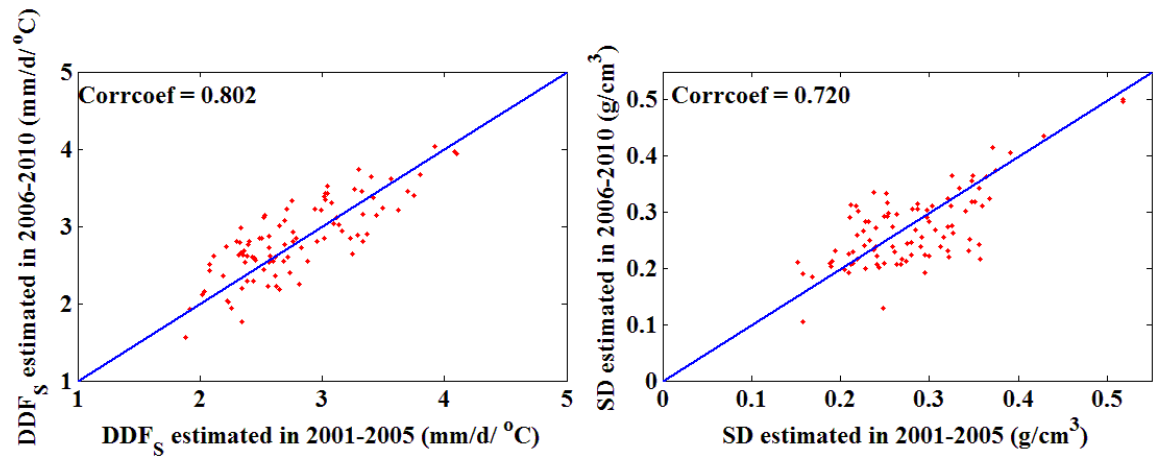
750

751 Figure 2. Spatial distribution of the snow density and the snowmelt degree-day factor (DDFs) estimated
 752 by the proposed method in the Lienz basin. Black dots indicate the stream gauges.



753
 754
 755
 756
 757

Figure 3. Snow density and snowmelt degree-day factor (DDF_s) estimated by the proposed method plotted against elevation in the Lienz basin. Each dot represents a sub-catchment in the basin. The size of dots increases with increasing of mean leaf area index (LAI) over the study period (2001-2010) which is derived from MODIS. LAI values in the basin range between 0.33 and 31.03.

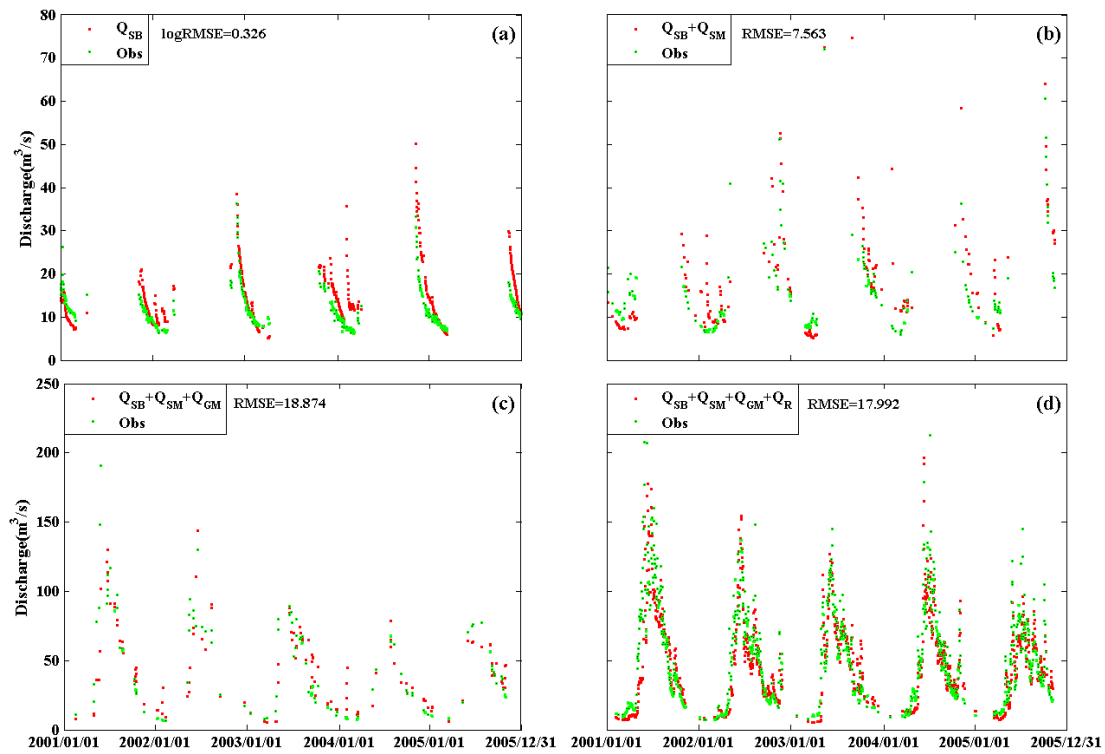


758

759

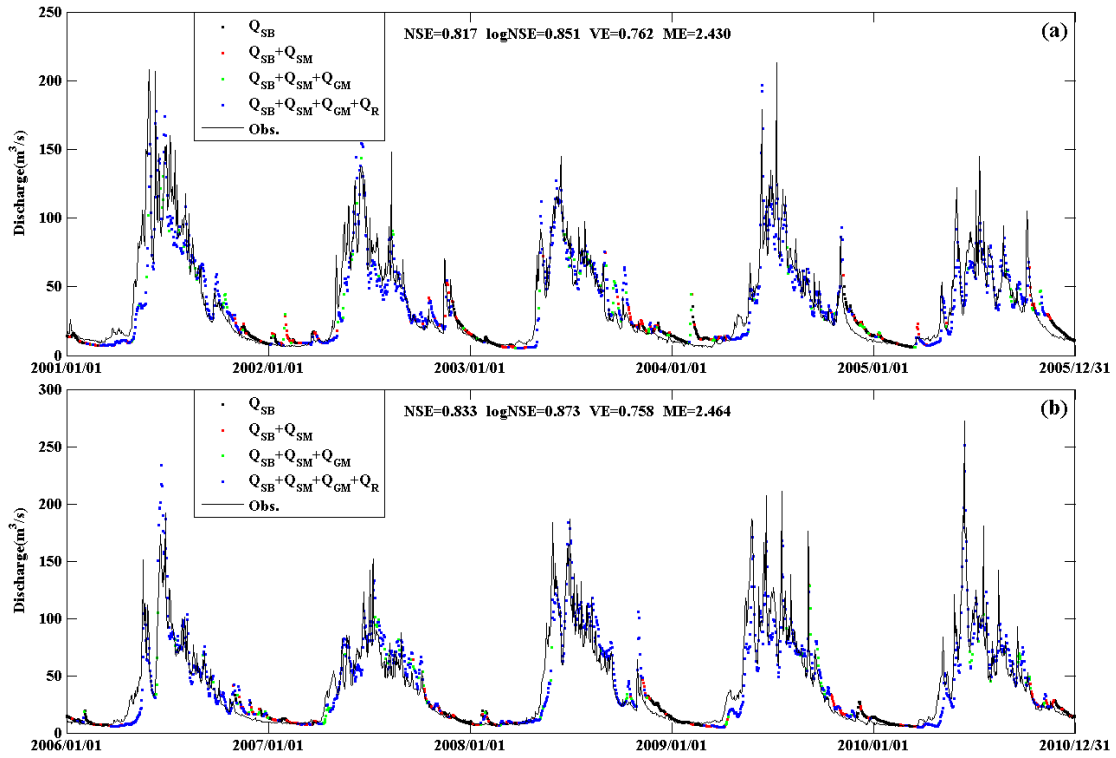
760

Figure 4. Comparison of the estimated degree-day factor for snowmelt (DDF_s) and snow density (SD) in two sub-periods. “Corrcoef” is the value of correlation coefficient between two estimated sets.



761
762
763
764
765
766

Figure 5. Stepwise calibration results for the Lienz basin in the calibration period. (a) is the first calibration step in which the parameters controlling groundwater baseflow are calibrated, (b) to (d) are the subsequent three steps of calibrating melt factors and rainfall runoff parameters. Q_{SB} , Q_{SM} , Q_{GM} and Q_R are the simulated discharges that are generated by baseflow, snowmelt, glacier melt and rainfall, respectively.



767

768

Figure 6. Simulation of daily discharge in the Lienz basin using the snowmelt degree-day factor calibrated on runoff. (a) is for the calibration period and (b) is for the validation period. The entire daily simulated discharge hydrograph has been combined from the simulations of different runoff segments.

770

771

772

773

Q_{SB} stands for the simulated runoff generated by groundwater baseflow, Q_{SM} and Q_{GM} indicate simulated runoff generated by snow and glacier melt, and Q_R is the simulated runoff generated by rainfall directly. Performance measures of the simulations are shown at the top of each panel.

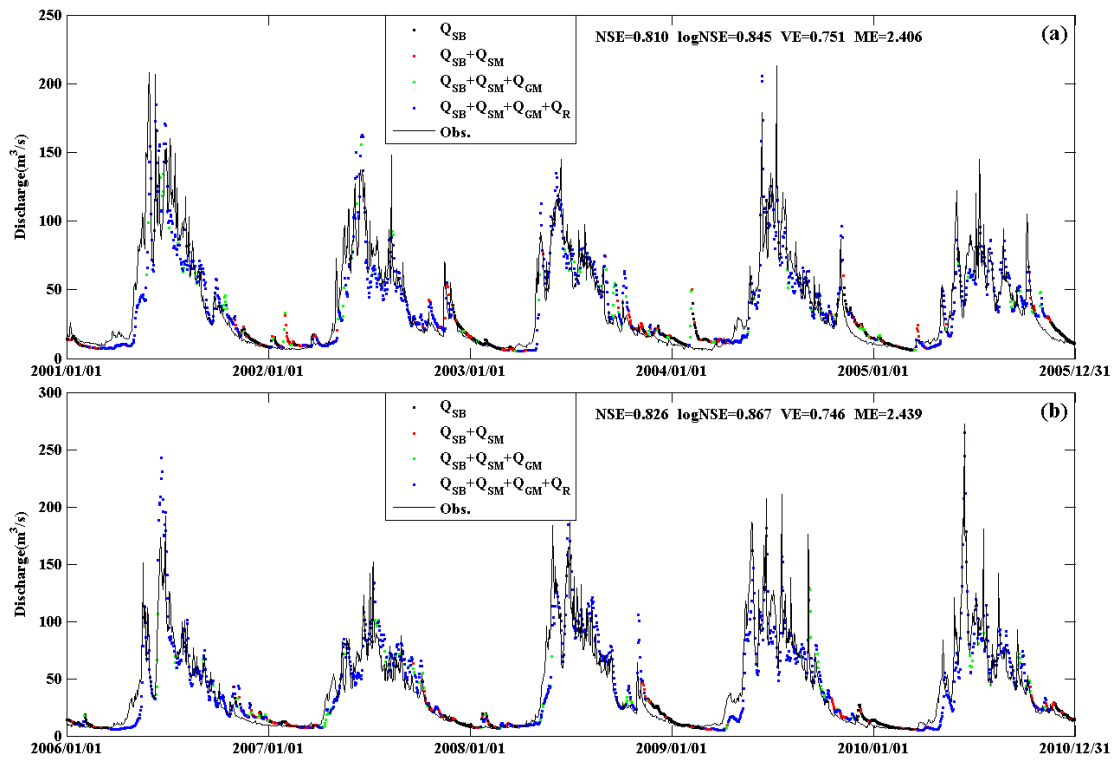
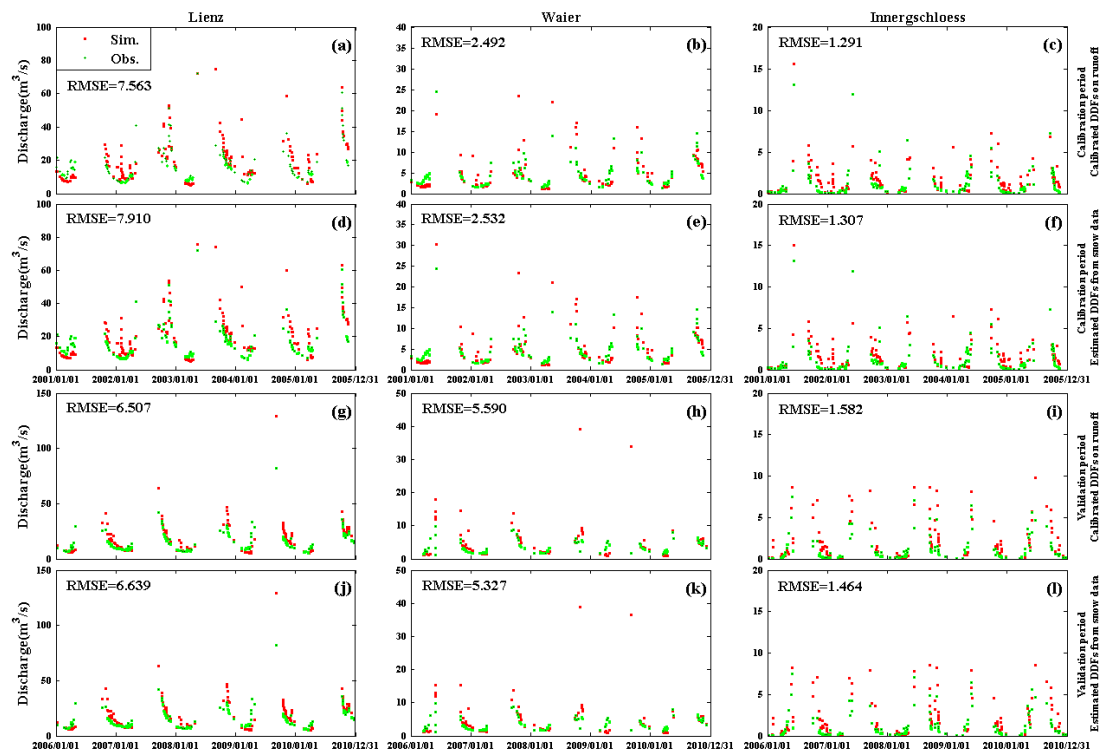
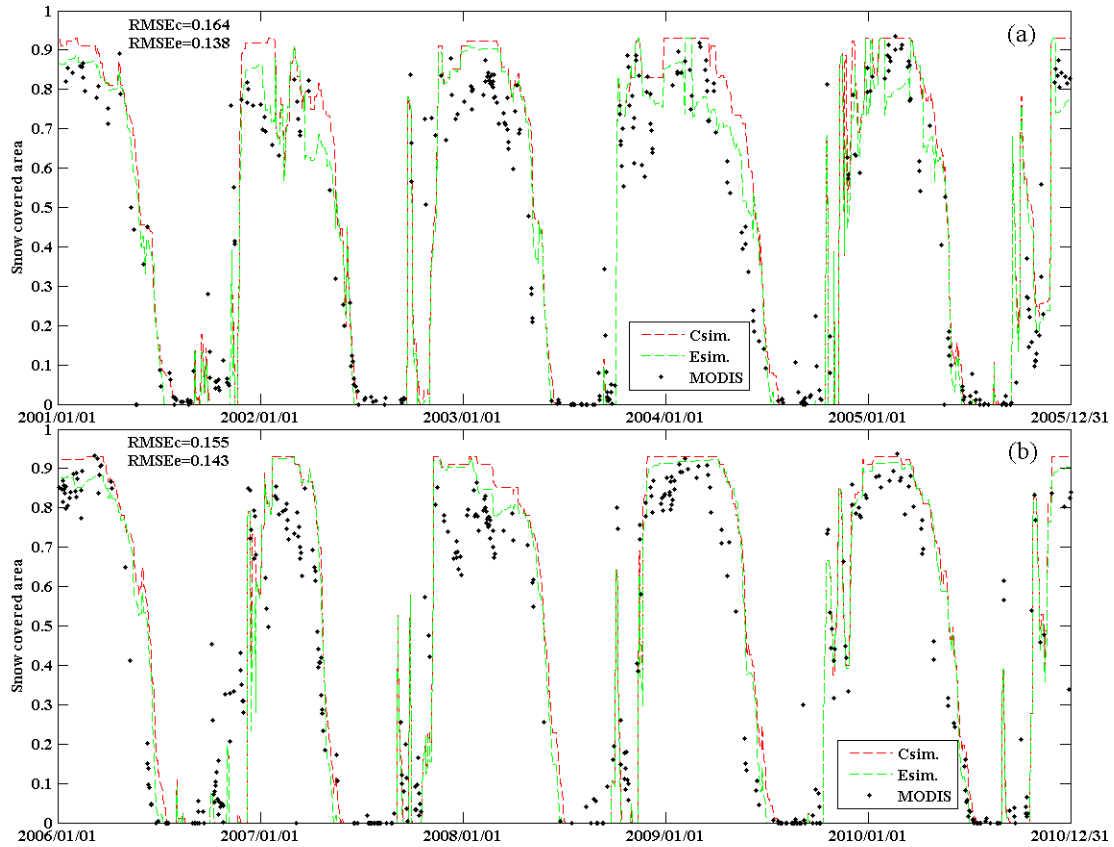


Figure 7. Same as Fig. 5 but using snowmelt degree-day factors estimated from snow data.



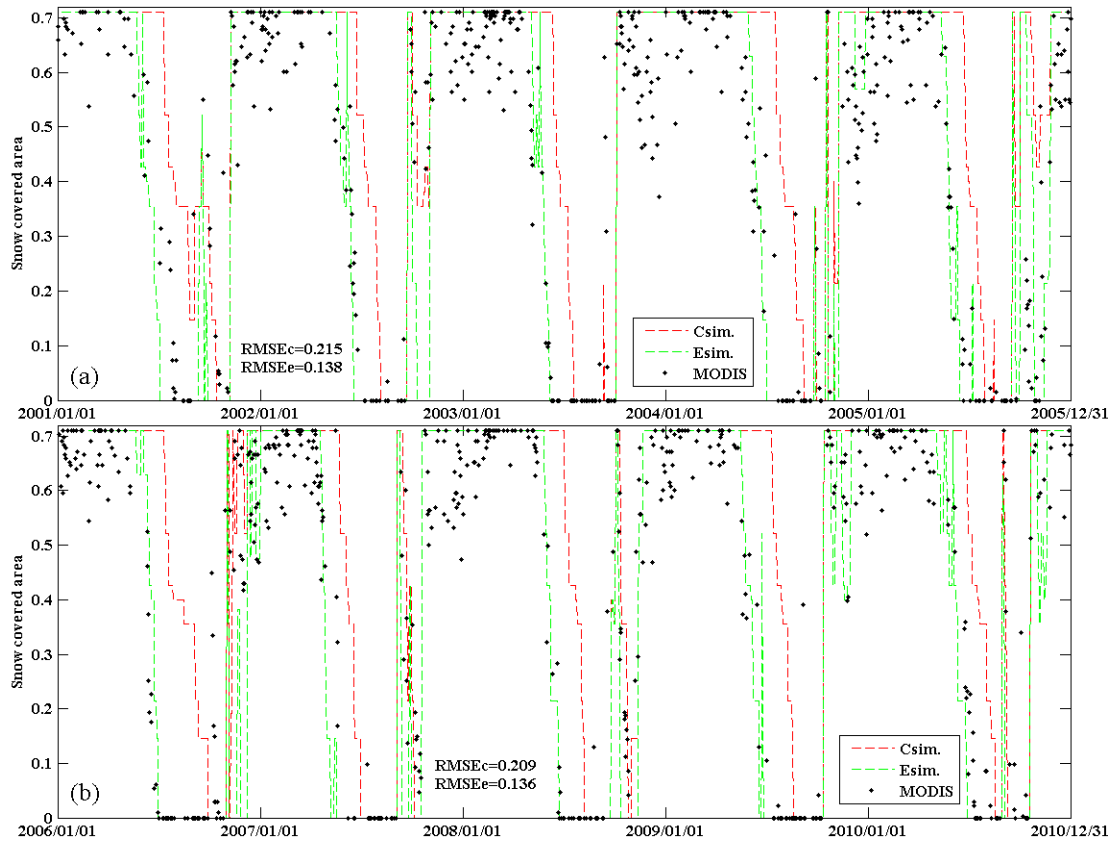
776
777
778
779
780
781
782

Figure 8. Simulations of discharge segments generated by groundwater baseflow (Q_{SB}) and snowmelt (Q_{SM}) in the three basins. (a)-(c) are simulations for the calibration period using DDF_S calibrated on runoff, (d)-(f) are simulation for the calibration period using DDF_S estimated from snow data, (g)-(i) are simulations for the validation period using DDF_S calibrated on runoff, (j)-(l) are simulations for the validation period using DDF_S estimated from snow data. The discharge simulations are evaluated using the $RMSE$ (m^3/s).



783

784 Figure 9. Simulations of the snow covered area (SCA) time series for the Lienz basin (1190 km²). Red
 785 lines (Csim.) represent the SCA simulation using the snowmelt degree-day factor (DDF_s) calibrated on
 786 runoff; green lines (Esim.) represent the SCA simulation using snowmelt degree-day factors estimated
 787 from snow data. Black dots are the MODIS observed SCA values. (a) is for the calibration period and
 788 (b) is for the validation period. The simulations are evaluated by *RMSE_c* for the calibrated DDF_s and
 789 *RMSE_e* for the estimated DDF_s.

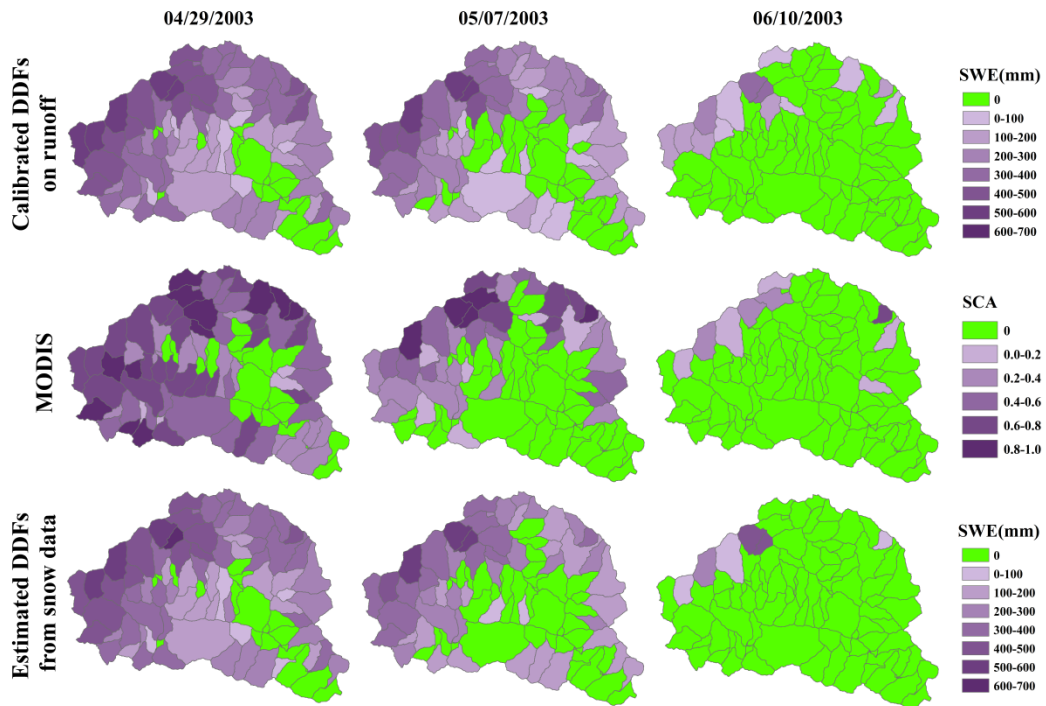


790

791

792

Figure 10. Same as Fig. 8 but for the Innerschloess basin (39 km²).



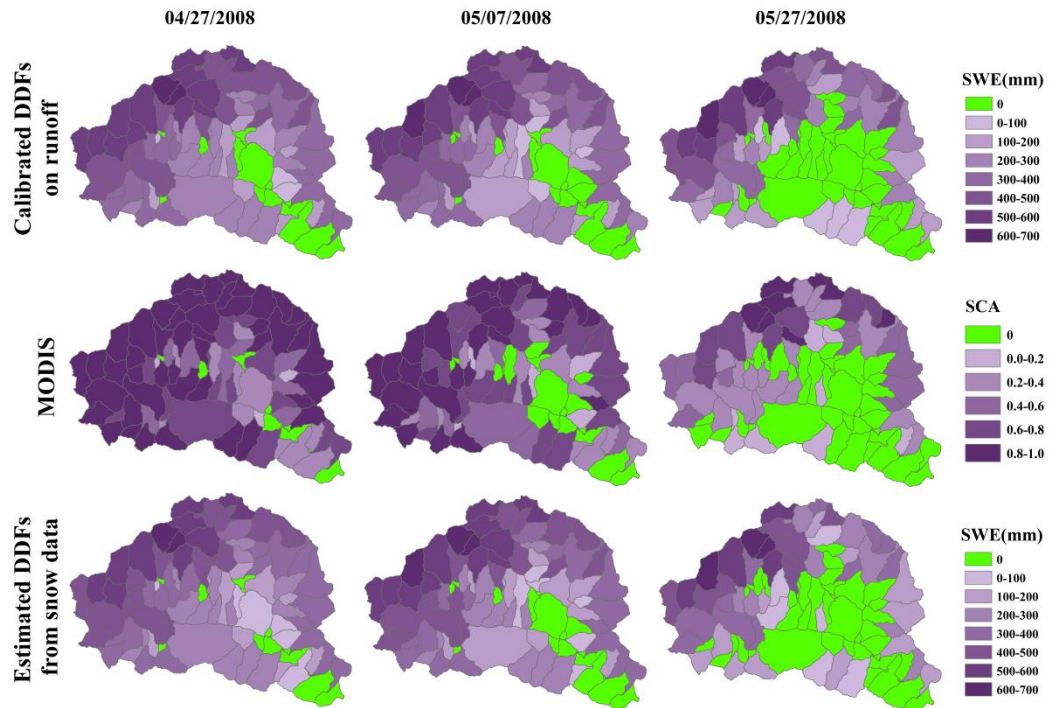
793

794 Figure 11. Simulations of snow patterns on three days within the calibration period (April 29th, May 7th

795 and June 10th, 2003). The top row shows simulated snow water equivalent (SWE) using DDF_s

796 calibrated on runoff, the middle row shows snow covered area (SCA) observed by MODIS, and the

797 bottom row shows simulated snow water equivalent using DDF_s estimated from snow data.



798

799 Figure 12. Same as Fig. 10 but for three days within the validation period (April 27th, May 7th and May

800

27th, 2008).